

## Global $\Lambda$ polarization in high energy collisions

Yilong Xie,<sup>1</sup> Dujuan Wang,<sup>2</sup> and László P. Csernai<sup>1</sup>

<sup>1</sup>*Institute of Physics and Technology, University of Bergen, Allegaten 55, 5007 Bergen, Norway*

<sup>2</sup>*School of Science, Wuhan University of Technology, 430070, Wuhan, China*

(Received 1 November 2016; published 14 March 2017)

With a Yang-Mills flux-tube initial state and a high-resolution (3+1)D particle-in-cell relativistic (PICR) hydrodynamics simulation, we calculate the  $\Lambda$  polarization for different energies. The origination of polarization in high energy collisions is discussed, and we find linear impact parameter dependence of the global  $\Lambda$  polarization. Furthermore, the global  $\Lambda$  polarization in our model decreases very quickly in the low energy domain, and the decline curve fits well the recent results of Beam Energy Scan (BES) program launched by the STAR Collaboration at the Relativistic Heavy Ion Collider (RHIC). The time evolution of polarization is also discussed.

DOI: [10.1103/PhysRevC.95.031901](https://doi.org/10.1103/PhysRevC.95.031901)

**Introduction.** The nontrivial polarization effect in high energy collisions, since it was first observed in Fermilab with both polarized and unpolarized incident beams [1,2], has been raising people's interest. The  $\Lambda$  hyperon is well suited to measure the polarization because through the decay  $\Lambda^0 \rightarrow p + \pi^-$  with proton carrying the spin information, the  $\Lambda$  becomes its own spin analyzer. Afterwards, more experimental research was launched continuously, including nucleon collisions and heavy ion collisions [3–9]. Theoretical studies have also been under way synchronously with the experiments [10–19].

These experiments have observed that (1) the  $\Lambda$  polarization is perpendicular to the reaction plane and (2) increases with the  $\Lambda$ 's transverse momentum ( $p_T$ ) and its Feynman  $x$ , taken to be  $x_F = p_L/\sqrt{s}$  [4,5,7]. However, no significant evidence was found to indicate the energy dependence of the hyperon polarization, which we will discuss in this Rapid Communication.

The  $\Lambda$  polarization in experiments was measured through the angular distribution of emitted protons in  $\Lambda$ 's rest frame:

$$\frac{dN}{d\cos\theta} = (1 + \alpha P \cos\theta)/4\pi, \quad (1)$$

where  $\theta$  is the angle between the proton momenta  $\mathbf{p}_p$  and the  $\Lambda$ 's spin  $\mathbf{S}_\Lambda$ ,  $P$  is the polarization amplitude, and the decay parameter  $\alpha$  is taken to be  $0.647 \pm 0.013$  [1,8]. To perform the measurement and calculation, it is crucial to determine the reaction plane (RP) and center of mass (c.m.) of the participant system. Recently it was pointed out that in collider experiments the c.m. frame determination might not be accurate enough due to the nuclear fragmentation effects, while the early fixed target experiments can get rid of this issue [20].

From these experiments, theorists have suggested that the hyperon polarization originates from the initial substantial angular momentum,  $L$ , in noncentral collisions, since the global polarization aligns with the orbital angular momentum. The initial angular momentum is dependent on impact parameter, or centrality percentage, taking a shape of quadratic function that peaks around 9% centrality percentage, as shown in Refs. [21,22]. In the RHIC's Au+Au collisions at 62.4 and 200 GeV, no centrality dependence of the global hyperon polarization was analyzed [23], due to the insignificant polarization.

Recently, stronger polarization signal was observed in RHIC's Beam Energy Scan (BES) program in the energy region below 100 GeV [24]. Therefore, in this Rapid Communication we will explore this issue again.

During past decades, two different perspectives were developed for the transition mechanism from initial angular momentum to the final state hyperon polarization, i.e., the hydrodynamical perspective and partonic kinetic perspective. From the partonic micro-perspective, the initial angular momentum is transferred to the partons through the interaction of spin-orbit coupling in viscous QGP [11], and then the global polarized quarks are recombined into hadrons, in which the Thomas precession of the quark spin was applied [25].

In the hydro- and thermodynamical description, the initial angular momentum is manifested in a longitudinal velocity shear, which, with small shear viscosity, results into a rotating system with substantial vorticity and even Kelvin-Helmholtz instability [26]. Assuming local equilibrium at freeze-out and equipartition of the spin degree of freedom, Ref. [15] put forward a polarization 3-vector for spin-1/2 particles and antiparticles based on the generalization of Cooper-Frye formula for particles with spin.

It was recently pointed out that the detailed balance of Cooper-Frye formula on freeze-out (FO) hypersurface requires a nonvanishing polarization in fluid before FO [27]. However, the absence of pre-FO polarization should not significantly affect the polarization calculation based on Ref. [15]. One can calculate that, the spin of each baryon is  $L = \hbar/2 \approx 98.5$  MeV fm/c. As the polarization is between 1 and 10% at different beam energies in the RHIC BES program, this gives  $L \approx 1$ –10 MeV fm/c for the angular momentum carried by one baryon. On the other hand the total angular momentum is around [28]:  $L = 1.05 \times 10^4 \hbar = 205.8 \times 10^4$  MeV fm/c. This is distributed among a few hundred baryons in semiperipheral reactions at not too high energies, i.e., very few antibaryons, which gives an angular momentum per baryon:  $L \approx 10^4$  MeV fm/c. This is 3 to 4 orders of magnitude bigger than the spin angular momentum carried by one baryon in the vortical flow. Therefore, even if 1–10% of spins are already polarized before FO, carrying only one per mil of the total angular momentum, they will neither effectively impact the fluid dynamical evolution, nor significantly change the detailed

balance during FO process, thus keeping the validity of the polarization 3-vector in Ref. [15].

References [17,18] applied this polarization 3-vector to relativistic heavy ion collisions to explore the momentum space distribution of  $\Lambda$  polarization. However, the previously neglected second term of the polarization formula, which reflects the effect of system expansion, turned out to be not negligible. In this Rapid Communication, we will compute the complete  $\Lambda$  polarization, including both the first and second terms, for the Au+Au collisions in the same energy domain as the RHIC BES program.

*$\Lambda$  polarization in hydrodynamic model.* The initial state we used here could naturally generate a longitudinal velocity shear [29,30], which leads to the hyperon polarization after the hydrodynamical evolution, simulated by a high-resolution computational fluid dynamic (CFD) calculation using the relativistic particle-in-cell (PICR) method. This initial state assumed a Yang-Mills field string tension between Lorentz contracted streaks after impact, and conserved the angular momentum both locally and globally. Both in the initial state and subsequent CFD simulation, the frequently used bag model equation of state (EoS) was applied:  $P = c_0^2 e^2 - \frac{4}{3} B$ , with constant  $c_0^2 = \frac{1}{3}$  and a fixed bag constant  $B$  [29–31]. The energy density takes the form  $e = \alpha T^4 + \beta T^2 + \gamma + B$ , where  $\alpha, \beta, \gamma$  are constants arising from the degeneracy factors for (anti)quarks and gluons. At freeze-out (FO) stage, the major part of FO hypersurface is assumed to be timelike, which entails small changes between the pre-FO and post-FO state, and thus the ideal gas phase space distribution can be applied [18,32].

The spatial part of polarization 3-vector for (anti) hyperon with mass  $m$  reads as [17–19]

$$\mathbf{\Pi}(p) = \frac{\hbar \varepsilon}{8m} \frac{\int d\Sigma_\lambda p^\lambda n_F (\nabla \times \boldsymbol{\beta})}{\int d\Sigma_\lambda p^\lambda n_F} + \frac{\hbar \mathbf{p}}{8m} \times \frac{\int d\Sigma_\lambda p^\lambda n_F (\partial_t \boldsymbol{\beta} + \nabla \beta^0)}{\int d\Sigma_\lambda p^\lambda n_F}, \quad (2)$$

where  $\beta^\mu(x) = (\beta^0, \boldsymbol{\beta}) = [1/T(x)]u^\mu(x)$  is the inverse temperature four-vector field, and  $n_F(x, p)$  is the Fermi-Jüttner distribution of the  $\Lambda$ , that is  $1/(e^{\beta(x) \cdot p - \xi(x)} + 1)$ , being  $\xi(x) = \mu(x)/T(x)$  with  $\mu$  being the  $\Lambda$ 's chemical potential and  $p$  its four-momentum.  $d\Sigma_\lambda$  is the freeze-out hypersurface element, for  $t = \text{const.}$  freeze-out,  $d\Sigma_\lambda p^\lambda \rightarrow dV \varepsilon$ , where  $\varepsilon = p^0$  is the  $\Lambda$ 's energy.

Here the *first term* reflects the classical vorticity effect ( $\nabla \times \boldsymbol{\beta}$ ), and the *second term* arises from the expansion effect ( $\partial_t \boldsymbol{\beta}$ ) and relativistic modification ( $\nabla \beta^0$ ). Noticing that the convention of  $\mathbf{\Pi}(p)$  is normalized to 50%, i.e., Eq. (1), the value should be multiplied by 2 to keep in line with the polarization anisotropy in experimental studies, where the upper limit is 100%. This is unlike the previous studies [13,17–19]. Besides, Eq. (2) is calculated in the center-of-mass (c.m.) frame, and one can Lorentz boost it into  $\Lambda$ 's rest frame by the following formula:

$$\mathbf{\Pi}_0(\mathbf{p}) = \mathbf{\Pi}(p) - \frac{\mathbf{p}}{p^0(p^0 + m)} \mathbf{\Pi}(p) \cdot \mathbf{p}. \quad (3)$$

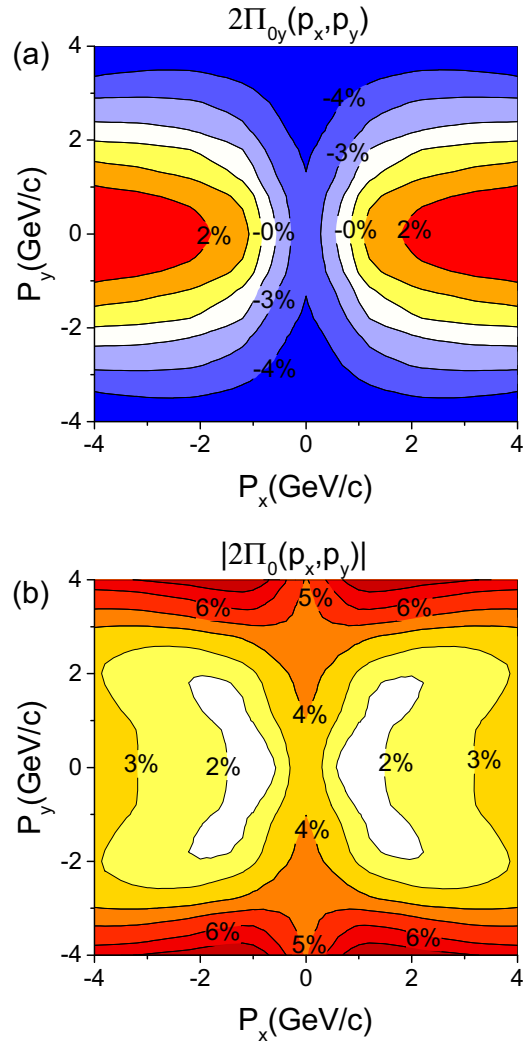


FIG. 1. The  $y$  component (top) and the modulus (bottom) of the  $\Lambda$  polarization for momentum vectors in the transverse,  $[p_x, p_y]$ , plane at  $p_z = 0$ , for the Au+Au reaction at  $\sqrt{s_{NN}} = 11.5$  GeV. The figure is in the frame of the  $\Lambda$ . The impact parameter  $b = 0.7b_m = 0.7 \times 2R$ , where  $R$  is the radius of Au and  $b_m = 2R$  is the maximum value of  $b$ . The freeze-out time is  $6.25 = (2.5 + 4.75)$  fm/c, including 2.5 fm/c for initial state and 4.75 fm/c for hydroevolution.

The three components of the polarization 3-vectors,  $2\Pi(p_x, p_y)$  [or  $2\Pi_0(p_x, p_y)$ ], have different significance. As we pointed out in our earlier paper [19], the  $x$  and  $y$  components of polarization,  $2\Pi_x$  and  $2\Pi_y$ , in transverse momentum space  $[p_x, p_y]$  are rather trivial and form a symmetric dipole structure, which results in vanishing global polarization along the  $x$  and  $y$  direction in the participant c.m. frame. Meanwhile, as expected, the  $-y$  directed polarization, aligned with the initial angular momentum, dominates the modulus of polarization 3-vector,  $2|\Pi_0(p_x, p_y)|$ . Figure 1 shows the dominant  $y$  component and the modulus of  $\Lambda$  polarization, in Au-Au collisions at 11.5 GeV. One can see that the top and bottom figures have similar structures and magnitudes, which indicates a trivial influence of the  $x$  and  $y$  components on the global polarization.

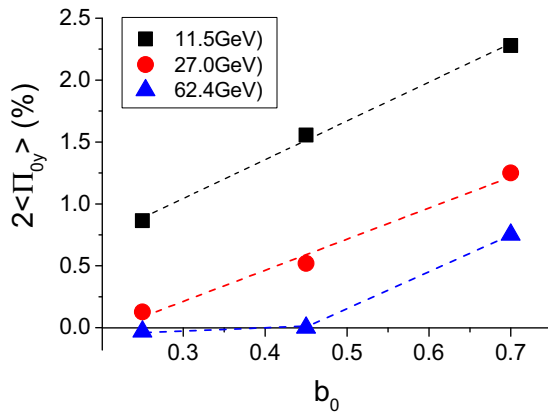


FIG. 2. The linear dependence of global polarization,  $2\langle \Pi_{0y} \rangle$ , as a function of impact parameter ratio  $b_0$  at 11.5, 27.0, and 62.4 GeV.

Since the  $-y$  directed global  $\Lambda$  polarization in experimental results is averaged polarization over the  $\Lambda$ 's momentum space, we evaluated the average of the  $y$  component of the polarization  $\langle \Pi_{0y} \rangle_p$ . We integrated the  $y$  component of the obtained polarization,  $\Pi_{0y}$ , over the momentum space as follows:

$$\begin{aligned} \langle \Pi_{0y} \rangle_p &= \frac{\int dp dx \Pi_{0y}(p, x) n_F(x, p)}{\int dp dx n_F(x, p)} \\ &= \frac{\int dp \Pi_{0y}(p) n_F(p)}{\int dp n_F(p)} \end{aligned} \quad (4)$$

to calculate the global polarization. The word *global* means averaging over phase space  $[x, p]$ . Besides, we replace the  $\langle \Pi_{0y} \rangle_p$  with  $-\langle \Pi_{0y} \rangle_p$ , since in experiments the angular momentum's direction, i.e., negative  $y$  direction, is the conventional direction for global polarization.

**Results and discussion.** According to the alignment of polarization and the system's angular momentum, theorists suggested attributing the polarization to the initial orbital angular momentum arising in noncentral collisions. References [21,22] have analytically deduced and schematically displayed the initial angular momentum in the reaction region as a function of impact parameter  $b$ , taking the form of quadratic function, which roughly peaks at  $b = 0.25b_m$  or  $0.3b_m$ . If the angular momentum is translated into polarization without any other significant perturbative mechanism, one should also observe the polarization's dependence on impact parameter. In other words, the initial angular momentum of the participant system is initiated by the inequality of local nuclear density in the transverse plane, and this inequality is dependent on the impact parameter. Thus the initial impact parameter dependence of the late-state polarization should in principle be observed.

Figure 2 shows the global polarization of Au+Au collisions as a function of ratio of impact parameter  $b$  to Au's nuclear radius  $R$ , i.e.,  $b_0 = b/2R$ . One could see that the polarization at different energies indeed approximately takes a linear increase with the increase of impact parameter, except for 62.4 GeV, due to the vanishing polarization signals at relatively central collisions. This linear dependence clearly indicates that the

polarization in our model arises from the initial angular momentum. However, the polarization's linear dependence on  $b$  is somewhat different from the angular momentum's quadratic dependence on  $b$ . This is because the angular momentum  $L$  is an extensive quantity dependent on the system's mass, while the polarization  $\Pi$  is an intensive quantity.

An earlier  $\Lambda$  global polarization measurement by the STAR Collaboration in Au+Au collisions at 62.4 and 200 GeV had observed an insignificant indication of centrality dependence, due to the occurrence of negative polarization, as well as large error bars [9,33]. The result of opposite directed global polarization at different centralities would be weird, if we assume that polarization comes from the angular momentum. Besides, no experimental  $\Lambda$  polarization measurements before the present ones had observed the opposite-pointing direction of global  $\Lambda$  polarization [1–6]. This might be because of the inappropriate choice of momentum space. However, from Figs. 5 and 7 in Refs. [9,33] one could still see that the polarization signal becomes stronger at larger centrality, while at small centrality percentage (below 40%) the signal is weak and vanishing. Similar behavior occurs in our simulation results for 62.4 GeV; specifically the polarization value also vanishes when the centrality percentage goes below 20% and increases as the centrality increases.

The recently reported global  $\Lambda$  polarization observation in STAR's BES I program has shown a positive signal for both  $\Lambda$  and  $\bar{\Lambda}$ , and thus it is promising to eliminate the disturbing opposite polarization direction that occurred in previous experiments [1–6], and this confirms our predictions. Besides, the RHIC's Event Plane Detector (EPD), on upgrading for future BES II with higher EP resolution, will provide a better chance to determine the issue of centrality dependence of  $\Lambda$  polarization [34]. With experimental c.m. identification one could also verify the momentum dependence of the polarization as shown in Fig. 1.

The  $\Lambda$  polarization increases with its Feynman  $x_F = p_L/\sqrt{s}$ , as well as transverse momentum  $p_T$ , had been observed in experiments and can be partly attributed to the

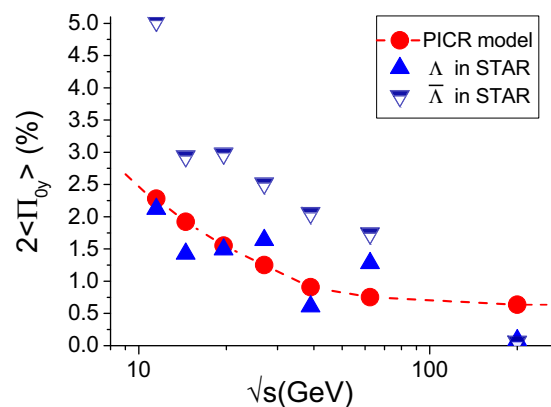


FIG. 3. The global polarization,  $2\langle \Pi_{0y} \rangle$ , in our PICR hydro-model (red circle) and STAR BES experiments (green triangle), at energies  $\sqrt{s}$  of 11.5, 14.5, 19.6, 27.0, 39.0, 62.4, and 200 GeV. The experimental data were extracted from Ref. [24], with solid triangle for  $\Lambda$  and hollow triangle for  $\bar{\Lambda}$ , dropping the error bars.

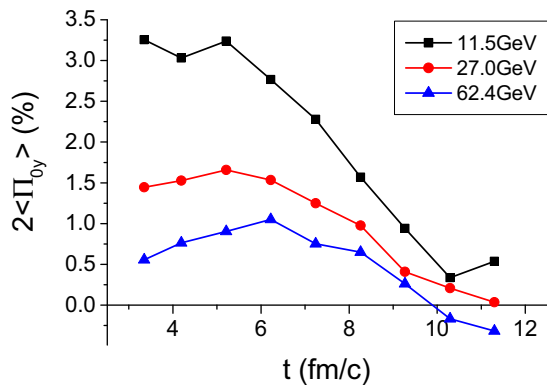


FIG. 4. The time evolution of global polarization,  $2\langle \Pi_{0y} \rangle_p$ , for energy  $\sqrt{s} = 11.5, 27$ , and  $62.4$  GeV.

$s\bar{s}$  pair production mechanism. It was also predicated that the polarization should also depend on the collision energy  $\sqrt{s}$ , although early experiments did not find evident signals to confirm this [4,5,7]. Recently with an exploration to low energy domain between  $7.7$  and  $27.0$  GeV, the RHIC BES I program had successfully observed the energy dependence of  $\Lambda$  polarization with a higher EP resolution and better background extraction.

Using the PICR hydrodynamical model, we calculated the global  $\Lambda$  polarization at the following energies:  $11.5, 14.5, 19.6, 27, 39, 62.4$ , and  $200$  GeV, and plotted them with red round symbols in Fig. 3. The impact parameter is  $b_0 = 0.7$ , i.e., the centrality is  $c = 49\%$ . For comparison the data of  $\Lambda$  and  $\bar{\Lambda}$  polarization from STAR (RHIC) were inserted into Fig. 3 with blue triangle symbols. One could see that our model fits fairly well the experimental data. Although the experimental  $\bar{\Lambda}$  polarization is larger than the  $\Lambda$  polarization, it will not change the averaged polarization very much, because the production ratio of  $\bar{\Lambda}$  to  $\Lambda$  is very small in high energy collisions [35].

Figure 3 clearly shows that  $\Lambda$  polarization is dependent on collision energy; it drops very quickly with increasing energy from  $11.4$  to  $62.4$  GeV and tends to saturate after  $62.4$  GeV. From a thermodynamical perspective, the polarization decreases with energy, and this can be attributed to the higher temperature in higher energy collisions. The drastic

thermal motion of particles will decrease the quark polarization rate, which according to Ref. [11] is inversely proportional to the collision energy. On the other hand, simulating results by a multi-phase transport (AMPT) model has shown that the averaged classical vorticity decreases with the collision energy [36,37], which, of course, leads to the decline of global  $\Lambda$  polarization.

It is also interesting to take a glance on the time evolution of  $\Lambda$  polarization, shown in Fig. 4. In this figure, the  $\Lambda$  polarization increases slowly at an early stage and then falls down very quickly. The negative polarization values that occur at  $62.4$  GeV after  $10$  fm/c demonstrate the loss of validity of the hydrodynamical model at late stages of system expansion, due to the large surface to volume ratio. Besides, at early stages, no  $\Lambda$ s are produced, so the climbing segment of the curves before  $4$  fm/c is not observable.

*Summary and conclusions.* With a Yang-Mills field initial state and a high resolution (3+1)D Particle-in-Cell Relativistic (PICR) hydrodynamics simulation, we calculate the  $\Lambda$  polarization for different low energies and different impact parameters. The polarization in high energy collisions originates from initial angular momentum or the inequality of local density between projectile and target, and both of them are sensitive to the impact parameter. Thus, we plotted the global polarization as a function of impact parameter  $b$  and a linear dependence on  $b$  was observed. We hope that after upgrading the Event Plane Detector, the STAR will provide higher resolution EP determination and centrality, to determine precisely the centrality dependence of global  $\Lambda$  polarization.

Furthermore, the global  $\Lambda$  polarization in our model decreases very quickly in the low energy domain, and the decline curve fits very well with the recent results of Beam Energy Scan (BES) program launched by STAR (RHIC). This is a very exciting new result, which indicates the significance of thermal vorticity and system expansion.

Finally, the time evolution of  $\Lambda$  polarization shows the limitation of hydrodynamical model at later stage of system expansion.

*Acknowledgments.* Enlightening discussions with Mike Lisa and Francesco Becattini are gratefully acknowledged. One of the authors, Y. L. Xie, is supported by the China Scholarship Council (China).

- 
- [1] G. Bunce, R. Handler, R. March, P. Martin, L. Pondrom, and M. Sheaff, *Phys. Rev. Lett.* **36**, 1113 (1976).  
[2] A. Lesnik, D. M. Schwartzf, I. Ambats, E. Hayes, W. T. Meyer, C. E. W. Ward, T. M. Knasel, E. G. Swallow, R. Winston, II, and T. A. Romanowski, *Phys. Rev. Lett.* **35**, 770 (1975).  
[3] M. Anikina *et al.*, *Z. Phys. C* **25**, 1 (1984).  
[4] A. M. Smith *et al.* (R608 Collaboration), *Phys. Lett. B* **185**, 209 (1987).  
[5] E. J. Ramberg *et al.*, *Phys. Lett. B* **338**, 403 (1994).  
[6] A. Morelos *et al.* (E761 Collaboration), *Phys. Rev. Lett.* **71**, 2172 (1993).  
[7] I. Abt *et al.* (HERA-B Collaboration), *Phys. Lett. B* **638**, 415 (2006).  
[8] I. Selyuzhenkov *et al.* (STAR Collaboration), *J. Phys. G: Nucl. Part. Phys.* **32**, S557 (2006).  
[9] B. I. Abelev *et al.*, *Phys. Rev. C* **76**, 024915 (2007).  
[10] Z.-T. Liang and X.-N. Wang, *Phys. Rev. Lett.* **94**, 102301 (2005).  
[11] X.-G. Huang, P. Huovinen, and X.-N. Wang, *Phys. Rev. C* **84**, 054910 (2011).  
[12] B. Betz, M. Gyulassy, and G. Torrieri, *Phys. Rev. C* **76**, 044901 (2007).  
[13] F. Becattini, G. Inghirami, V. Rolando, A. Beraudo, L. D. Zanna, A. De Pace, M. Nardi, G. Pagliara, and V. Chandra, *Eur. Phys. J. C* **75**, 406 (2015).  
[14] A. D. Panagiotou, *Phys. Rev. C* **33**, 1999 (1986).  
[15] F. Becattini, V. Chandra, L. Del Zanna, and E. Grossi, *Ann. Phys.* **338**, 32 (2013).

- [16] C. C. Barros and Y. Hama, *Int. J. Mod. Phys. E* **17**, 371 (2008).
- [17] F. Becattini, L. P. Csernai, and D. J. Wang, *Phys. Rev. C* **88**, 034905 (2013).
- [18] Y.-L. Xie, R. C. Glastad, and L. P. Csernai, *Phys. Rev. C* **92**, 064901 (2015).
- [19] Y. L. Xie, M. Bleicher, H. Stöcker, D. J. Wang, and L. P. Csernai, *Phys. Rev. C* **94**, 054907 (2016).
- [20] L. P. Csernai, G. Eyyubova, and V. K. Magas, *Phys. Rev. C* **86**, 024912 (2012).
- [21] F. Becattini, F. Piccinini, and J. Rizzo, *Phys. Rev. C* **77**, 024906 (2008).
- [22] J.-H. Gao, S.-W. Chen, W.-T. Deng, Z.-T. Liang, Q. Wang, and X.-N. Wang, *Phys. Rev. C* **77**, 044902 (2008).
- [23] I. Karpenko and F. Becattini, [arXiv:1610.04717](https://arxiv.org/abs/1610.04717).
- [24] M. A. Lisa *et al.* (STAR Collaboration), QCD Chirality Workshop 2016, Feb. 23–26, 2016, Los Angeles, USA (unpublished).
- [25] T. A. DeGrand and H. I. Miettinen, *Phys. Rev. D* **24**, 2419 (1981).
- [26] L. P. Csernai, D. D. Strottman, and Cs. Anderlik, *Phys. Rev. C* **85**, 054901 (2012).
- [27] D. Montenegro, L. Tinti, and G. Torrieri, [arXiv:1701.08263](https://arxiv.org/abs/1701.08263) (unpublished).
- [28] L. P. Csernai, D. J. Wang, and T. Csorgo, *Phys. Rev. C* **90**, 024901 (2014).
- [29] V. K. Magas, L. P. Csernai, and D. D. Strottman, *Phys. Rev. C* **64**, 014901 (2001).
- [30] V. K. Magas, L. P. Csernai, and D. D. Strottman, *Nucl. Phys. A* **712**, 167 (2002).
- [31] L. P. Csernai, *Introduction to Relativistic Heavy Ion Collisions* (Jonh Wiley & Sons Ltd., Chichester, UK, 1994).
- [32] Y. Cheng, L. P. Csernai, V. K. Magas, B. R. Schlei, and D. D. Strottman, *Phys. Rev. C* **81**, 064910 (2010).
- [33] R.-H. Fang, L.-G. Pang, Q. Wang, and X.-N. Wang, *Phys. Rev. C* **94**, 024904 (2016).
- [34] J.-L. Zhang *et al.* (STAR Collaboration), Strangeness in Quark Matter 2016, June 27–July 1, 2016, Berkeley, USA (unpublished).
- [35] T. Anticic *et al.* (NA49 Collaboration), *Phys. Lett. B* **93**, 022302-1 (2004).
- [36] Y. Jiang, Z.-W. Lin, and J.-F. Liao, *Phys. Rev. C* **94**, 044910 (2016).
- [37] W.-T. Deng and X.-G. Huang, *Phys. Rev. C* **93**, 064907 (2016).